Sonochemical Synthesis of A Novel Nanoscale 1D Lead(II) $[Pb_2(L)_2(I)_4]_n$ Metal-Organic Coordination Polymer, Survey of Temperature and Reaction Time Parameters

Payam Hayati [c,a], Salvio Suárez-García [c], Angel Gutiérrez[d], Daniel Ruiz Molina[c*], Ali Morsali[b*], Ali Reza Rezvani[a*]

[a] Department of Chemistry, Faculty of Sciences, University of Sistan and Baluchestan, P.O. Box 98135-674, Zahedan, Iran.

[b] Department of Chemistry, Faculty of Sciences, Tarbiat Modares University, P.O. Box 14115-4838, Tehran, Islamic Republic of Iran.

[c] Catalan Institute of Nanoscience and Nanotechnology (ICN2), CSIC and BIST, Campus UAB, Bellaterra, 08193 Barcelona, Spain.

[d] Departamento de Química Inorgánica I Facultad de Ciencias Químicas, Universidad Complutense, 28040 Madrid, Spain.

Abstract

One new lead coordination supramolecular complex (CSC) (1D), $[Pb_2(L)_2(I)_4]_n$, L= $C_4H_6N_2$ (1-methyl imidazole), has been synthesized under different experimental conditions. Micrometric crystals (bulk) or nano-sized materials have been obtained depending on using the branch tube method or sonochemical irradiation. All materials have been characterized by scanning electron microscopy (SEM), powder X-ray diffraction (PXRD) and FT-IR spectroscopy. Single crystal X-ray analyses on complex **1** showed that Pb^{2+} ion is 4-coordinated. Topological analysis shows that the complex **1** is 2,3,5C2 net. Finally, the role of reaction time and temperature on the growth and final morphology of the structures obtained by sonochemical irradiation have been studied.

Keywords: Coordination polymer, Sonochemical process, Ultrasound irradiation, Morphology.

1. Introduction

During the past two decades, the rational design, construction, and characterization of metal–organic coordination polymers (CPs) have received significant attention in the fields of materials chemistry and crystal engineering, owing to intriguing structures and potential applications in a variety of fields such as luminescence [1, 2], magnetism [3-5], gas absorption and separation, chemical sensors [6-8], heterogeneous catalysis [9-11] and drug delivery [12, 13]. Although a great number of coordination polymers with diverse structures and interesting properties have been constructed, the precise prediction and controllable preparation of such materials are still a great challenge for chemists, since a lot of factors may largely affect the overall structural formation. The metal-organic networks or coordination polymers based on lead(II) remain less explored, mostly due to the toxicity of this metal, as well as its somewhat unpredictable coordination behavior. Actually, the electronic configuration of Pb(II) allows the Pb^{2+} cation showing a large variety of coordination numbers and geometries. However, interest in the coordination polymers of lead has recently substantially increased. This is presumably related to the diversity of coordination modes of the metal and the unique supramolecular architectures of such complex [14-17]. Several unique synthetic approaches have already been offered for the preparation of coordination complex. Some of them are (1) slow diffusion of the reactants into a polymeric matrix, (2) diffusion from the gas phase, (3) evaporation of the solvent at ambient or reduced pressures, (4) precipitation or recrystallization from a mixture of solvents, (5) temperature controlled cooling and (6) hydrothermal synthesis [18-22]. However, the traditional approaches must be carried out at high temperatures (373–523 K) and pressures (1–10 MPa) with long reaction times [23]. In contrast to the traditional energy sources, ultrasonic irradiation is regarded as a facile and environmentally friendly energy source, which could provide rather

unusual reaction conditions (a short duration of extremely high temperatures and pressures in liquids) [24–26]. These extreme conditions can drive chemical reactions and then promote the formation of nano-structure materials. The nano-sized particles of CPs often exhibit superior properties that cannot be seen in bulk crystals because they are controlled by a large surface-to-volume ratio [27, 28]. So, the syntheses of nanostructures are important for the development of science and technology within the nanoscale realm [29, 30]. However the sonochemical methods have been adopted for preparation of nanomaterials, the application of the ultrasonic method for construction of CPs receives relatively limited attention [31–37]. Until now, only examples of $[Pb(ind)_2(H_2O)]_n$, $[Pb_2(dbsf)_2(bipy)]_n$ (Hind = indane-2-carboxylic acid, H_2dbsf = 4,4′-sulfonyldibenzoic acid, bipy 4,4′-bipyridine) [38], $[Pb_2(mpic)_4(H_2O)]\cdot 0.5H_2O$, $[Pb_2(phen)_2(cit)(mes)]\cdot 2H_2O$, mpic=3-methyl picolinate, phen= *o*-phenanthroline, H_2cit=citraconic acid, H_2mes mesaconic acid. [39], $[Pb_3(tmph)_4(\mu\ N_3)_5(\mu\text{-}NO_3)]_n$,tmph=3,4,7,8-tetramethyl-1,10-phenanthroline)[40], $[Pb_3(BOABA)_2(H_2O)]\cdot H_2O\}_n$, $\{[Pb_4(BOABA)_2(\mu_4\text{-}O)(H_2O)_2]\cdot H_2O\}_n$, H_3BOABA=3,5-bis-oxyacetate-benzoic acid) [41], $[Pb(L)(\mu_2\text{-}I)]_n$, L = 1H-1,2,4-triazole-3-carboxylate [42], $[Pb(tmph)(\mu\text{-}SCN)_2]_n$, $[Pb(tmph)(\mu\text{-}NO_3)_2]_n$, tmph = 3,4,7,8-tetramethyl-1,10-phenanthroline) [43], $[Pb_2(Hcpip)_2(ox)]_n$, $[Pb_2(Hcpip)_2(suc)]_n$, H_2ox = oxalic acid, H_2suc = succinic acid,) [44],$[Pb(qcnh)(NO_3)_2]_n$, qcnh = 2-quinolincarbaldehyde nicotinohydrazide [45], rare lead (II) coordination polymer complex with different ligand are reported. However, the synthesis of lead-based 1D coordination polymers still represents a challenge. Herein, we report the synthesis of a novel nanoscale 1D lead(II) coordination polymer with ultrasounds method. We will demonstrate that this is a robust process independent of experimental parameters such as temperature and reaction time. Moreover, crystal suitable for x-

ray diffraction of the same complex have been obtained by the branched tube method and successfully compared with the x-ray diffraction of sonochemical samples.

2. Experimental

2.1. Materials and physical techniques

Starting reagents for the synthesis were purchased and used without any purification from industrial suppliers (Sigma–Aldrich, Merck and others). Elemental analyses (carbon, hydrogen, and nitrogen) were performed employing a Heraeus Analytical Jena, Multi EA 3100 CHNO rapid analyzer. Fourier transform infrared spectra were recorded on a Bruker Tensor 27 FT-IR with a single window reflection of diamond ATR (Attenuated total reflectance) model MKII with the OPUS as data collection software. The instrument was equipped with a room temperature detector, and a mid-IR source (4000 to 400 cm^{-1}). Since it is a single beam instrument, it was needed to run a background spectrum in air before the measurement. Single crystal X-ray diffraction (SXRD) experiments were carried out for complex **1** with MoKα radiation (λ=0.71073 Å) at ambient temperature. A micro focused Rigaku mm003 source with integrated confocal caxFlux double bounce optic and HPAD Pilatus 200K detector was used for **1** while for two data were measured on a Bruker-Nonius Kappa CCD diffractometer. The structures were solved by direct methods and refined by full matrix least squares on F^2. All non-hydrogen atoms were refined anisotropically. The hydrogen atoms were included with fixed isotropic contributions at their calculated positions determined by molecular geometry, except for the oxygen bonded hydrogen atoms, which were located on a difference Fourier map and refined riding on the corresponding atoms. (Computing details: data collection, cell refinement and data reduction: CrystalClear-SM expert 2.1b43 [46]; program(s) used to solve structure: SHELXT [47]; program(s) used to refine structure: SHELXL-2014/7; molecular graphics:

PLATON [48]; reduction of data and semiempirical absorption correction: SADABS program[49]; direct methods (SIR97 program[50]); full-matrix least-squares method on F^2: SHELXL-97 program [51] with the aid of the programs WinGX [52] and Olex2[53]. A complete structure solution, refinement and analysis program [54)]. Powder X-ray diffraction (PXRD) measurements were performed using an X'pert diffractometer manufactured by Philips with monochromatized Cukα radiation and simulated PXRD patterns based on single crystal data were prepared using the Mercury software [53]. The samples were characterized with a scanning electron microscope (SEM) (FEI Quanta 650 FEG) in mode operation of secondary electrons (SE) with a beam voltage between 15 and 20 KV. The samples were prepared by deposition of a drop of the material previously dispersed in properly solvents on aluminum stubs followed by evaporation of the solvent under ambient conditions. Before performing the analysis, the samples were metalized by depositing on the surface a thin platinum layer (5 nm) using a sputter coater (Leica EM ACE600). A multi wave ultrasonic generator (Elmasonic (Elma) S40 H), equipped with a converter/transducer and titanium oscillator (horn), 12.5 mm in diameter, operating at 20 kHz with a maximum power output of 400 W, were used for the ultrasonic irradiation.

2.8. Synthesis of $[Pb_2(L)_2(I)_4]_n$ (2) as single crystals

$Pb(NO_3)_2$ (1 mmol, 0.331g), 1-methlimidazole (L) (2 mmol, 0.15ml) and KI (2 mmol, 332g) were loaded into one arm of a branch tube and both of the arms were filled slowly with methanol. The chemical bearing arm was immersed in an oil bath kept at 60 °C. Crystals were formed on the inside surface of the arm kept at ambient temperature. After 10 days, yellow crystals were deposited in the cooler arm, filtered off, washed with methanol and air dried. (0.104 g, 38.37 %, yield based on final product), complex **1** (single crystal): m.p >300 °C. Anal.

Calc. for $Pb_4I_8N_8C_{16}H_{24}$: C: 8.83, H: 1.10, N: 5.15 %; Found C: 8.21 H: 1.05, N: 5.12 %. IR (selected bands for complex **1**; in cm^{-1}):3115(w), 2479(br), 1530(s), 1529.40(s), 1507(s).

2.9. Synthesis of $[Pb_2(L)_2(I)_4]_n$ (1) under ultrasonic irradiation

To prepare the nano-/microstructures of $[Pb_2(L)_2(I)_4]_n$ **(1)** by sonochemical process, a high-density ultrasonic probe immersed directly into the solution of $Pb(NO_3)_2$ (10 ml, 0.1 M) in water, then into this solution, a proper volume of KI (10 ml, 0.1 M) and 1-methylimidazole (L) (10 ml, 0.1 M) ligand in water solvent was added in a drop wise manner. The solution was irradiated by ultrasound with the power of 60W and temperature 30 °C and after 30 min a yellow powder was obtained (complex **1-1**, temperature: 30°C reaction time: 30 min, sonication power: 60W, concentration: 0.1 M). For the study of the effect of temperature, the described process was done increasing the temperature to 60°C (complex **1-2**, reaction time: 30 min, sonication power: 60W, concentration: 0.1 M), and for the study of the effect of reaction time, it was increased up to 60 min (complex **1-3**, temperature: 30°C, sonication power: 60W, concentration: 0.1 M). The obtained precipitates were filtered, subsequently washed with water and then dried.

Complex **1-1**: (0.125 g, 46.12 %, yield based on final product), complex **1-1**: m.p >300 °C. Anal. Calc. for $Pb_4I_8N_8C_{16}H_{24}$: C: 8.83, H: 1.10, N: 5.15 %; Found C: 8.20 H: 0.99, N: 5.05 %. IR (selected bands for complex **1-1**; in cm^{-1}): 3110(w), 2460(br), 1529(s), 1505(s), 1265(s).

Complex **1-2**: (0.118 g, 43.54 %, yield based on final product), complex **1-2**: m.p >300 °C. Anal. Calc. for $Pb_4I_8N_8C_{16}H_{24}$: C: 8.83, H: 1.10, N: 5.15 %; Found C: 8.61 H: 1.00, N: 5.14 %. IR (selected bands for complex **1-2**; in cm^{-1}): 3108(w), 2429(br), 1522(s), 1501(s), 1269(s), cm^{-1}.

Complex **1-3**: (0.134 g, 49.44 %, yield based on final product), complex **1-3**: m.p >300 °C. Anal. Calc. for $Pb_4I_8N_8C_{16}H_{24}$: C: 8.83, H: 1.10, N: 5.15 %; Found C: 8.76 H: 1.04, N: 5.06 %. IR (selected bands for complex **1-3**; in cm^{-1}): 3119(w), 2481(br), 1528(s), 1509(s), 1266(s).

3. Results and discussion

3.1. Single crystal x-ray diffraction (SXRD)

Crystal suitable for x-ray diffraction was obtained from solution by thermal gradient method applied to an aqueous and methanol solution of the reagents (the "branched tube method"). Reaction of L= $C_4H_6N_2$ (1-methyl imidazole), potassium iodide with lead(II) nitrate in methanol induce the formation of the new 1D coordination polymer $[Pb_2(L)_2(I)_4]_n$ **(1)**. Single crystal X-ray diffraction analysis (Tables 1- 2) of complex **1** was carried out and the coordination environment of the titled complexes. $[Pb_2(L)_2(I)_4]_n$ **(1)** complex crystallize in a triclinic space group P_{-1}. The Pb atoms of complex **1** are coordinated by five I atoms and one N atom composing octahedral I_5N (Fig. 1). The asymmetric unit of complex **1** contains two Pb^{2+} cations, which coordinate to two 1-methyl imidazole ligands (L) and four I^- anions (Fig. 2). Each 1-methyl imidazole (L) ligand in complex **1** is coordinated to one Pb atom by N atom of pyridine ring (Hg-N distance of 2.428 Å). Additionally, there are two type of I atoms around the Pb atoms: axial and equatorial I atoms are coordinated to each Pb atom with contacts distances $Pb–I_{ax}$ and $Pb-I_{eq}$ of 3.421 and 3.210 Å, respectively (Table 3 and Fig. 3). It should be noted that the intramolecular and intermolecular interactions can be separated in two groups: strong (more valence) in short range 0.93-3.72 Å; and weak (more electrostatic) in long range 3.18-4.45 Å. Strong bonds form mononuclear complexes $[Pb(L)(I)_3]$, which expanded by relatively weak interactions in polymeric chains $[Pb_2(L)_2(I)_4]_n$ along translation *a* axis (Fig 4). On the other hand, there is $\pi - \pi$

interaction between aromatic rings which lead to crystal structure be stable and distance between two aromatic rings is 4.552 Å (Fig. 5 and 6). It should be noted, that each chain in the network is surrounded by six other ones, producing hexagonal shape of growth for the network (Fig.7 and 8). Simplification of the chain to the underlying net by ToposPro package reveals 2,3,5C2 topological type, which is abundant for 1D coordination polymers (Fig. 9) (more than 100 examples in TTO collection of ToposPro) [55-56].

3.2. Hirshfeld surface analysis

In order to analyze the various interactions those lead to the crystal structure, a study of the Hirshfeld surface was performed. In this study, the volume of space where molecule electron density exceeds all neighboring molecules was considered [57-59]. Molecular Hirshfeld surfaces have been constructed from CIF file, for this reason structures can be dissected into noncovalent contacts [60-64]. The very high-resolution Hirshfeld surfaces were generated by Crystal Explorer and functions of curvature, distance including shape index and dnorm were mapped to the surfaces [60-64]. The function d_{norm} is a normalized distance property defined by d_i(distance from a point on the Hirshfeld surface to the nearest internal nucleus), d_e (distance from a point on the Hirshfeld surface to the nearest external nucleus) and van der Waals radii (r_i^{vdW} and r_e^{vdW}), being: $d_{norm}= [(d_i - r_i^{vdW})/r_i^{vdW}]+[(d_e - r_e^{vdW})/r_e^{vdW}]$ [22-24]. Thus, the value of d_{norm} was negative or positive when intermolecular contacts were shorter or longer than r^{vdW}, respectively. The Hirshfeld surfaces of the titled complex (Fig. 10) were mapped over a d_{norm}, de, d_i, curvedness and shape-index.

The d_{norm} values were mapped to the Hirshfeld surface (Fig 10a) by using a red – blue – white color scheme as follows: red regions represented closer contacts as well as a negative d_{norm} value; blue regions represented longer contacts and a positive d_{norm} value; and white regions represented

the distance of contacts equal to precisely the van der Waals separation with a d_{norm} value of zero. These normalized contact distances (d_{norm}) reveal the close contacts of valence bond donors and acceptors, but other close contacts are evident. As shown in Fig 15a the large circular depressions are the indicators of valence bonding contacts and the dominant interactions are Pb-I, whereas other visible spots are due to π-π interactions, based on both d_e and d_i. Particularly, adjacent red/orange and blue triangle like patches on a shape index map (Fig-11) give us information about valence bond and π-π interactions [60, 63-64]. The combination of the distances from the Hirshfeld surface to the nearest nucleus inside the surface (d_i) and outside the surface (d_e) and the data conveyed by the shape index are consistent with 2D fingerprint plots [58-59].

The 2D fingerprint maps of **1** provide some quantitative information giving the possibility of obtaining additional insight to the intermolecular interactions in the crystal state and for describing the surface characteristics of the molecules (Fig. 12). Globally, I……H, H……H, Pb……I and H…..C intermolecular interactions were most abundant in the crystal packing (45.3%, 19.2%, 17.1% and 8.4%, respectively). It really is evident that van der Waals forces exert an important influence on the stabilization of the packing in the crystal structure, and other intercontacts [N……H/H…….N (5.6%), Pb…..H (1%), I……C (1.4%), N……C (0.1%) and C……C (0.4%)] contribute less to the Hirshfeld surfaces. On the other hand, the relative contributions of the different interactions to the Hirshfeld Surfaces were also calculated for the title complex (Fig. 13).

3.2. Sonochemical synthesis

Synthesis of complex **1** was alternatively achieved by the application of ultrasounds. For the synthesis of complex **1**, a high-density ultrasonic probe was immersed directly into a water solution $Pb(NO_3)_2$ and posterior drop wise addition a second methanol solution of KI and 1-methyl imidazole (**L**). The synthesis were done keeping constant the reactants concentration (0.1 M) and the ultrasound power (60 W) while other factors such as temperature and the reaction time were systematically modified (a resume of the different reactions is shown in Table 3, for more details see section 2.9).

In order to confirm the coordination of the different complexes synthesized, FT-IR measurements were performed (Fig. 14). The absorption bands with variable intensity in the frequency range around 3100 cm^{-1} correspond to N-H symmetric stretching frequency of the 1-methyl imidazole ligand, absorption bands around 2790 cm^{-1} are related to CH_3 symmetric bending frequency. Additionally, aromatic C-H stretching frequency appears at around 3035 cm^{-1}. The absorption bands with variable intensity in the frequency range 1560-1640 cm^{-1} correspond to N-H bending frequency of the amine group of the 1-methyl imidazole ligand. The absorption bands around 1300 cm^{-1} are attributed to symmetry bending frequency of the CH_3 group.

Powder X-ray diffraction (PXRD) of complexes **1-1**, **1-2** and **1-3** (see Figure 15) revealed that all of them exhibit the same crystalline phase which in turns is also similar to that obtained upon simulation from the X-ray diffraction data obtained for **1**. These results indicate the existence of a single crystalline phase, which is maintained independently of the synthesis method as well as of the temperature (30ºC and 60ºC) and reaction times (30 min and 60 min). Similar results are

obtained as far as the morphology of the nanocrystal is considered. The morphology and size of products prepared by the sonochemical method and observed by SEM images showed the formation of needles for all the reactants (Fig. 16). Moreover, the variation of temperature and the reaction time in the ultrasounds did not affect the morphology neither the crystalline phase of the complex. SEM images of complexes **1-1** to **1-3** had the same needle morphology (Fig. 16a, b, c). Bravais Friedel Donnay Harker (BFDH) analysis was carried out in order to estimate the faces that are supposed to appear in the crystals morphology. This analysis considers the effect of symmetry operations on the interplanar distances of crystal faces. Predicted crystal morphology of complex **1** is shown in Fig. 16d. In almost all cases, there is a good match between the predicted and observed morphology. It should be noted that in the case of **1**, the growth of the coordination material takes place along the [00-1] direction (Fig. 16e). It is interesting to note, that the shape of chains parallel to chain orientation in the structure is quite similar to the morphology of cross section to long axes for needle-like crystals. However the relation between crystallographic orientation of the chains and the faces of the crystals needs further study.

4. Conclusions

Sonochemical methods have been used to obtain crystalline rods a few micron length and nanometers width of the 1D coordination polymer $[Pb_2(L)_2(I)_4]_n$. Larger crystals suitable for single crystal x-ray diffraction have been obtained by the branched tube method. Interestingly, the simulated x-ray diffraction powder obtained from the x-ray data confirms the structure of the nano-/microcrystal obtained by sonochemistry. These results confirm the potentially of ultrasound for the obtaining of nanoscale coordination polymers. The robustness of the reaction was confirmed and validated by repeating the reaction under different experimental conditions where the temperature and reaction time have been modified.

Supplementary material

Crystallographic data for the structure reported in this paper have been deposited with the Cambridge Crystallographic Data Centre as supplementary publication no. CCDC-1515619. Copies of the data can be obtained upon application to CCDC, 12 Union Road, Cambridge CB2 1EZ, UK (Fax: +44 1223/336033; e-mail: deposit@ccdc.cam.ac.uk).

Acknowledgement

This work was supported by grant MAT 2015-70615-R from the Spanish Government and by Feder funds. Funded by the CERCA Program / Generalitat de Catalunya. ICN2 is supported by the Severo Ochoa program from Spanish MINECO (Grant No. SEV-2013-0295).

References:

[1] A.C. Wibowo, S.A. Vaughn, M.D. Smith, H.-C. zur Loye, Novel bismuth and lead coordination polymers synthesized with pyridine-2, 5-dicarboxylates: two single component "white" light emitting phosphors, Inorganic chemistry, 49 (2010) 11001-11008.

[2] O. Toma, N. Mercier, M. Bouilland, M. Allain, N-oxide-4, 4′-bipyridine, a forgotten ligand in coordination chemistry: structure–photoluminescence property relationships in 2D and 1D lead-coordination polymers, CrystEngComm, 14 (2012) 7844-7847.

[3] M. Kurmoo, Magnetic metal–organic frameworks, Chemical Society Reviews, 38 (2009) 1353-1379.

[4] H. Fukunaga, H. Miyasaka, Magnet Design by Integration of Layer and Chain Magnetic Systems in a π Stacked Pillared Layer Framework, Angewandte Chemie, 127 (2015) 579-583.

[5] C.-L. Chang, X.-Y. Qi, J.-W. Zhang, Y.-M. Qiu, X.-J. Li, X. Wang, Y. Bai, J.-L. Sun, H.-W. Liu, Facile synthesis of magnetic homochiral metal–organic frameworks for "enantioselective fishing", Chemical Communications, 51 (2015) 3566-3569.

[6] L.E. Kreno, K. Leong, O.K. Farha, M. Allendorf, R.P. Van Duyne, J.T. Hupp, Metal–organic framework materials as chemical sensors, Chem. Rev, 112 (2012) 1105-1125.

[7] Z. Hu, B.J. Deibert, J. Li, Luminescent metal–organic frameworks for chemical sensing and explosive detection, Chemical Society Reviews, 43 (2014) 5815-5840.

[8] J.-N. Hao, B. Yan, A water-stable lanthanide-functionalized MOF as a highly selective and sensitive fluorescent probe for Cd 2+, Chemical Communications, 51 (2015) 7737-7740.

[9] J. Lee, O.K. Farha, J. Roberts, K.A. Scheidt, S.T. Nguyen, J.T. Hupp, Metal–organic framework materials as catalysts, Chemical Society Reviews, 38 (2009) 1450-1459.

[10] M. Yoon, R. Srirambalaji, K. Kim, Homochiral metal–organic frameworks for asymmetric heterogeneous catalysis, Chemical reviews, 112 (2011) 1196-1231.

[11] K. Manna, T. Zhang, F.X. Greene, W. Lin, Bipyridine-and phenanthroline-based metal–organic frameworks for highly efficient and tandem catalytic organic transformations via directed C–H activation, Journal of the American Chemical Society, 137 (2015) 2665-2673.

[12] M. Arıcı, O.Z. Yeşilel, S. Keskin, O. Şahin, Gas adsorption/separation properties of metal directed self-assembly of two coordination polymers with 5-nitroisophthalate, Journal of Solid State Chemistry, 210 (2014) 280-286.

[13] W.J. Rieter, K.M. Pott, K.M. Taylor, W. Lin, Nanoscale coordination polymers for platinum-based anticancer drug delivery, Journal of the American Chemical Society, 130 (2008) 11584-11585.

[14] F. Marandi, M. Mottaghi, G. Meyer, I. Pantenburg, Subtle Interplay of Weak Intermolecular Interactions. Crystal Structures of Lead (II) Complexes with 4, 4′-Dimethyl-2, 2′-bipyridine, Zeitschrift für anorganische und allgemeine Chemie, 635 (2009) 165-170.

[15] F. Marandi, S. Chantrapromma, H.-K. Fun, Synthesis and spectroscopic studies of mixed-ligand complexes of lead (II) hexafluoroacetylacetonate including the crystal structure of $[Pb_2(phen)_4(hfa)_2$ (Journal of Coordination Chemistry, 62 (2009) 249-256.

[16] F. Marandi, R. Rutvand, M. Rafiee, J.H. Goh, H.-K. Fun, Synthesis, properties and crystal structures of new binuclear lead (II) complexes based on phenyl, naphthyl-containing fluorine β-diketones and substituted 2, 2′-bipyridines, Inorganica Chimica Acta, 363 (2010) 4000-4007.

[17] S. Taheri, F. Marandi, H.K. Fun, R. Kia, $\{[Pb(PDT)_4][PbBr_3]_2\}_n$: Aggregation of Novel Discrete Cationic Lead (II) Complexes with an Anionic 1D Coordination Polymer, Zeitschrift für anorganische und allgemeine Chemie, 635 (2009) 1352-1354.

[18] A.K. Hall, J.M. Harrowfield, A. Morsali, A.A. Soudi, A. Yanovsky, Bonds and lone pairs in the flexible coordination sphere of lead (II), CrystEngComm, 2 (2000) 82-85.

[19] C. Janiak, A critical account on π–π stacking in metal complexes with aromatic nitrogen-containing ligands, Journal of the Chemical Society, Dalton Transactions, (2000) 3885-3896.

[20] K. Akhbari, A. Morsali, Silver nanofibers from the nanorods of one-dimensional organometallic coordination polymers, CrystEngComm, 12 (2010) 3394-3396.

[21] T.M. Barclay, A.W. Cordes, J.R. Mingie, R.T. Oakley, K.E. Preuss, A bis (1, 2, 3-dithiazole) charge transfer salt with 2: 1 stoichiometry; inhibition of association and generation of slipped-stacks, CrystEngComm, 2 (2000) 89-91.

[22] C.A. Hunter, J.K. Sanders, The nature of. pi.-. pi. interactions, Journal of the American Chemical Society, 112 (1990) 5525-5534.

[23] Y. Hanifehpour, V. Safarifard, A. Morsali, B. Mirtamizdoust, S.W. Joo, Ultrasound-assisted fabrication of a new nano-rods 3D copper (II)-organic coordination supramolecular compound, Ultrasonics sonochemistry, 31 (2016) 201-205.

[24] N. Soltanzadeh, A. Morsali, Sonochemical synthesis of a new nano-structures bismuth (III) supramolecular compound: new precursor for the preparation of bismuth (III) oxide nano-rods and bismuth (III) iodide nano-wires, Ultrasonics sonochemistry, 17 (2010) 139-144.

[25] N.A. Dhas, K.S. Suslick, Sonochemical preparation of hollow nanospheres and hollow nanocrystals, Journal of the American Chemical Society, 127 (2005) 2368-2369.

[26] Y. Hanifehpour, A. Morsali, B. Soltani, B. Mirtamizdoust, S.W. Joo, Ultrasound-assisted fabrication of a novel nickel (II)-bis-pyrazolyl borate two-nuclear discrete nano-structured coordination compound, Ultrasonics sonochemistry, 34 (2017) 519-524.

[27] J.H. Bang, K.S. Suslick, Applications of ultrasound to the synthesis of nanostructured materials, Advanced materials, 22 (2010) 1039-1059.

[28] M.J.S. Fard-Jahromi, A. Morsali, Sonochemical synthesis of nanoscale mixed-ligands lead (II) coordination polymers as precursors for preparation of $Pb_2(SO_4)O$ and PbO nanoparticles; thermal, structural and X-ray powder diffraction studies, Ultrasonics sonochemistry, 17 (2010) 435-440.

[29] Z. Shan, E. Stach, J. Wiezorek, J. Knapp, D. Follstaedt, S. Mao, Grain boundary-mediated plasticity in nanocrystalline nickel, Science, 305 (2004) 654-657.

[30] Y. Hirai, K. Nakabayashi, M. Kojima, M. Atobe, Size-controlled spherical polymer nanoparticles: Synthesis with tandem acoustic emulsification followed by soap-free emulsion polymerization and one-step fabrication of colloidal crystal films of various colors, Ultrasonics sonochemistry, 21 (2014) 1921-1927.

[31] K. Akhbari, A. Morsali, Two-dimensional thallium (I) supramolecular polymer constructed from Tl⋯ π interactions: a new precursor for the preparation of thallium (III) oxide with a nano-structural surface, Polyhedron, 30 (2011) 1456-1462.

[32] K. Akhbari, M. Hemmati, A. Morsali, Fabrication of silver nanoparticles and 3D interpenetrated coordination polymer nanorods from the same initial reagents, Journal of Inorganic and Organometallic Polymers and Materials, 21 (2011) 352-359.

[33] K. Akhbari, S. Beheshti, A. Morsali, G. Bruno, H.A. Rudbari, How the two factors of concentration and ultrasonic wave power affect on formation of kinetically or thermodynamically stable lead (II) complex nano-structures, Inorganica Chimica Acta, 423 (2014) 101-105.

[34] S. Hojaghani, K. Akhbari, M.H. Sadr, A. Morsali, Sonochemical syntheses of one-dimensional silver (I) supramolecular polymer: a precursor for preparation of silver nanostructure, Inorganic Chemistry Communications, 44 (2014) 1-5.

[35] E. Mirzadeh, K. Akhbari, A. Phuruangrat, F. Costantino, A survey on the effects of ultrasonic irradiation, reaction time and concentration of initial reagents on formation of kinetically or thermodynamically stable copper (I) metal-organic nanomaterials, Ultrasonics sonochemistry, 35 (2017) 382-388.

[36] F. Shahangi Shirazi, K. Akhbari, S. Kawata, R. Ishikawa, Effects of different factors on the formation of nanorods and nanosheets of silver(I) coordination polymer, J. Mol. Struct. 1123 (2016) 206‑212.

[37] M. Moeinian, K. Akhbari, J. Boonmak, S. Youngme, Similar to what occurs in biological systems; irreversible replacement of potassium with thallium in coordination polymer nanostructures, Polyhedron, 118 (2016) 6-11.

[38] D. Hazari, S.K. Jana, H. Puschmann, E. Zangrando, S. Dalai, 1D lead (II) coordination chains with carboxylate containing ligands. A rare example of polyrotaxane 1D→1D interpenetrated coordination polymer, Inorganic Chemistry Communications, 65 (2016) 1-3.

[39] A. Rana, S.K. Jana, S. Datta, R.J. Butcher, E. Zangrando, S. Dalai, 1D coordination polymers formed by tetranuclear lead (II) building blocks with carboxylate ligands: In situ isomerization of itaconic acid, Journal of Solid State Chemistry, 207 (2013) 61-68.

[40] Y. Hanifehpour, A. Morsali, B. Mirtamizdoust, S.W. Joo, Sonochemical synthesis of tri-nuclear lead (II)-azido nano rods coordination polymer with 3, 4, 7, 8-tetramethyl-1, 10-phenanthroline (tmph): Crystal structure determination and preparation of nano lead (II) oxide, Journal of Molecular Structure, 1079 (2015) 67-73.

[41] Y.-Q. Chen, Y. Tian, Lead (II) coordination polymers based on rigid-flexible 3, 5-bis-oxyacetate-benzoic acid: Structural transition driven by temperature control, Journal of Solid State Chemistry, 247 (2017) 60-66.

[42] V. Safarifard, A. Morsali, Sonochemical syntheses of nano lead (II) iodide triazole carboxylate coordination polymer: precursor for facile fabrication of lead (II) oxide/iodide nano-structures, Inorganica Chimica Acta, 398 (2013) 151-157.

[43] Y. Hanifehpour, V. Safarifard, A. Morsali, B. Mirtamizdoust, S.W. Joo, Sonochemical syntheses of two new flower-like nano-scale high coordinated lead (II) supramolecular coordination polymers, Ultrasonics sonochemistry, 23 (2015) 282-288.

[44] Q.-H. Bao, Q. Chen, H.-M. Hu, Y.-L. Ren, B. Xu, F.-X. Dong, M.-L. Yang, G.-L. Xue, Hydrothermal synthesis and crystal structure of four lead (II) coordination polymers with a carboxylate functionalized imidazophenanthroline derivative ligand, Inorganica Chimica Acta, 405 (2013) 51-57.

[45] B. Mirtamizdoust, Z. Trávníček, Y. Hanifehpour, P. Talemi, H. Hammud, S.W. Joo, Synthesis and characterization of nano-peanuts of lead (II) coordination polymer [Pb (qcnh)$(NO_3)_2$] n with ultrasonic assistance: A new precursor for the preparation of pure-phase nano-sized PbO, Ultrasonics sonochemistry, 34 (2017) 255-261.

[46] Rigaku (2014) CrystalClear-SM expert 2.1b43 The Woodlands, Texas, USA, and Rigaku Corporation, Tokyo, Japan.

[47] Sheldrick, G. M. (2015). Acta Cryst. A71, 3-8.

[48] Spek, A. L. (2009). Acta Cryst. D65, 148–155.

[49] SADABS, Bruker-Nonius, Delft, The Netherlands, 2002.

[50] A. Altomare, M. C. Burla, M. Camalli, G. L. Cascarano, C. Giacovazzo, A. Guagliardi, G. G. Moliterni, G. Polidori, R. Spagna, J. Appl. Crystallogr. 32 (1999) 115-119.

[51] G. M. Sheldrick, Acta Crystallogr. A64 (2008) 112-122.

[52] L. J. Farrugia, J. Appl. Crystallogr. 45 (2012) 849-854.

[53] Mercury 1.4.1, Copyright Cambridge Crystallographic Data Centre, 12 Union Road, Cambridge, CB2 1EZ, UK, 2001–2005.

[54] O.V. Dolomanov, L.J. Bourhis, R.J. Gildea, J.A. Howard, H. Puschmann, OLEX2: a complete structure solution, refinement and analysis program, Journal of Applied Crystallography, 42 (2009) 339-341.

[55] V.A. Blatov, A.P. Shevchenko, D.M. Proserpio, Applied topological analysis of crystal structures with the program package ToposPro, Crystal Growth & Design, 14 (2014) 3576-3586.

[56] E.V. Alexandrov, V.ABlatov, A.Kochetkov, D.M. Proserpio, Underlying nets in three-periodic coordination polymers: topology, taxonomy and prediction from a computer-aided analysis of the Cambridge Structural Database, CrystEngComm, 13 (2011) 3947-3958.

[57] N. Cnesn, C. W. Worne, Crystal Habit of Synthetic Ghalcanthite (Copper Sulfate Pentahydrate) as Related to Position and Orientation in Growth Solution, Am. Mineral., 59 (1974) 1105-1112.

[58] O. Urgut, I. Ozturk, C. Banti, N. Kourkoumelis, M. Manoli, A. Tasiopoulos, S. Hadjikakou, New antimony (III) halide complexes with dithiocarbamate ligands derived from thiuram degradation: the effect of the molecule's close contacts on in vitro cytotoxic activity, Materials Science and Engineering: C, 58 (2016) 396-408.

[59] O. Urgut, I. Ozturk, C. Banti, N. Kourkoumelis, M. Manoli, A. Tasiopoulos, S. Hadjikakou, Addition of tetraethylthiuram disulfide to antimony (III) iodide; synthesis, characterization and biological activity, Inorganica Chimica Acta, 443 (2016) 141-150.

[60] M.A. Spackman, J.J. McKinnon, Fingerprinting intermolecular interactions in molecular crystals, CrystEngComm, 4 (2002) 378-392.

[61] E. Bouaziz, C.B. Hassen, N. Chniba-Boudjada, A. Daoud, T. Mhiri, M. Boujelbene, Crystal structure, Hirshfeld surface analysis, vibrational, thermal behavior and UV spectroscopy of (2, 6-Diaminopyridinium) dihydrogen arsenate, Journal of Molecular Structure, (2017).

[62] D. Jayatilaka, J. McKinnon, M. Spackman, Towards quantitative analysis of intermolecular interactions with Hirshfeld surfaces, Chem. Commun., (2007) 3814.

[63] M.A. Spackman, D. Jayatilaka, Hirshfeld surface analysis, CrystEngComm, 11 (2009) 1932.

[64] Rodrigo S. Bitzer, Lorenzo C. Visentin, Manfredo Horner, Marco A.C. Nascimento, Carlos A.L. Filgueiras ; J. Mol. Struct, 1130 (2017) 165.

Table 1. Crystal data and structures refinement for $[Pb_2(L)_2(I)_4]_n$ **(1)**

Empirical formula	**$Pb\ I\ N_2\ C_4\ H_6$**
Formula weight	**543.10 g/mol**
Temperature	**293(2)K**
Wavelength	**0.71073 Å**
Crystal system	**Triclinic**
Space group	P_{-1}
Unit cell dimensions	**a = 4.5520(2)Å,α =104.796(1)°**
	b = 12.4614(5)Å, β = 92.902(1)°
	c = 12.893 (3)Å,γ =71.778 (9)°
Volume	**1001.99 (7) $Å^3$**
Z	**4**
Density(calculated)	**3.600 g/cm^3**
Absorption coefficient	**22.934 Mg/m^3**
F(0 0 0)	**928**
Theta range for data collection	**1.1 to 31.9°**
μ	**22.93 mm^{-1}**
Index ranges	**$-6 \leq h \leq 6$**
	$-17 \leq k \leq 17$
	$-17 \leq l \leq 17$
(sin θ/λ)max	**0.744 $Å^{-1}$**
Theta(max)	**31.9°**
Radiation type	**Mo Kα**
Refinement method	**Full–matrix least–squares on F^2**
Goodness- of- fit on F^2	**1.042**
Refinement	**$R[F^2 > 2\sigma(F^2)]=0.030$**
	$wR(F^2)=0.057$
	S=1.13
	24099, 6412, 5072
Rint	**0.026**
Largest diff. peak and hole	**1.29, -1.24 eA^{-3}**
CCDC no.	**1515619**

Table 2. Selected bond lengths (Å) for complex $[Pb_2(L)_2(I)_4]_n$ **(1)**

Pb(1)—N(1)	2.428(5)	Pb(2)—I(3)	3.2407(5)
Pb(1)—I(1)^{i}	3.1647(5)	Pb(2)—I(3)^{i}	3.2491(5)
Pb(1)—I(4)^{i}	3.2026(5)	Pb(2)—I(4)	3.4212(5)
Pb(1)—I(1)	3.2322(5)	I(4)—Pb(1)^{ii}	3.2026(5)
Pb(1)—I(4)	3.2698(5)	I(1)—Pb(1)^{ii}	3.1648(5)
Pb(2)—N(3)	2.474(5)	I(2)—Pb(2)^{i}	3.1873(5)
Pb(2)—I(2)^{ii}	3.1873(5)	I(3)—Pb(2)^{ii}	3.2492(5)
Pb(2)—I(2)	3.2102(5)	N(1)—C(1)	1.324(8)

Symmetry transformations used to generate equivalent atoms:

(i) 1+x, y, z; (ii) -1+x, y, z.

Table 3. Resume of the different sonochemical reactions done, where the temperature and the reaction time have been systematically modified. In all the cases, ultrasounds power was 60 W.

Complex	M(mol/l)[a]	T (°C)[b]	t (min)[c]
1-1	0.1	30	30
1-2	0.1	60	30
1-3	0.1	30	60

[a] Concentration of initial reactant; [b] Reaction temperature; [c] Reaction time;

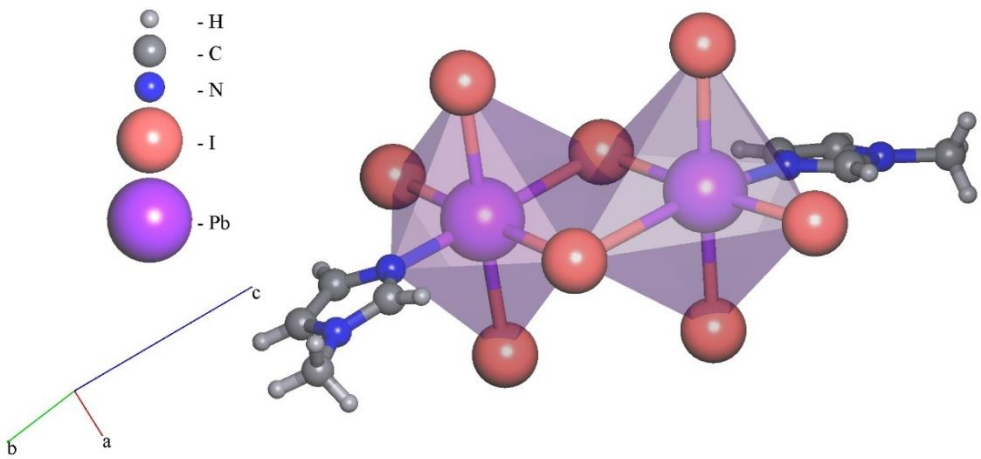

Figure 1. Coordination environment of Pb^{+2} cations in complex **1**.

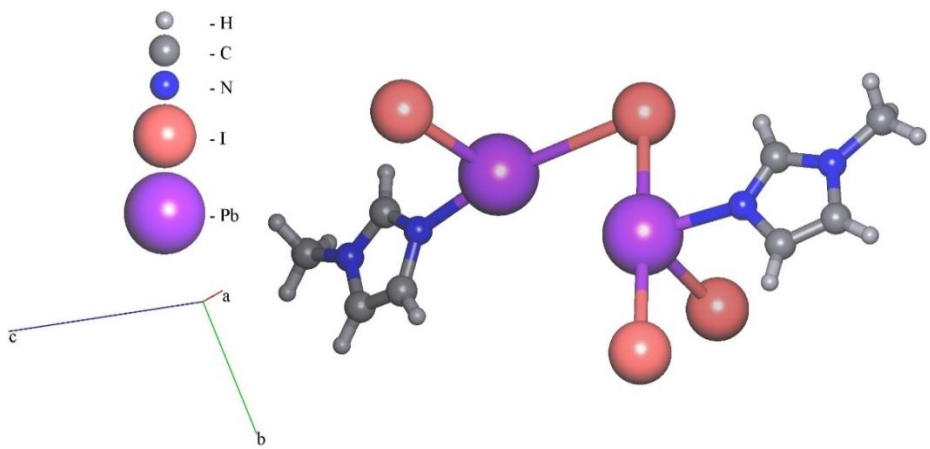

Figure 2. Asymmetric unit of complex **1**.

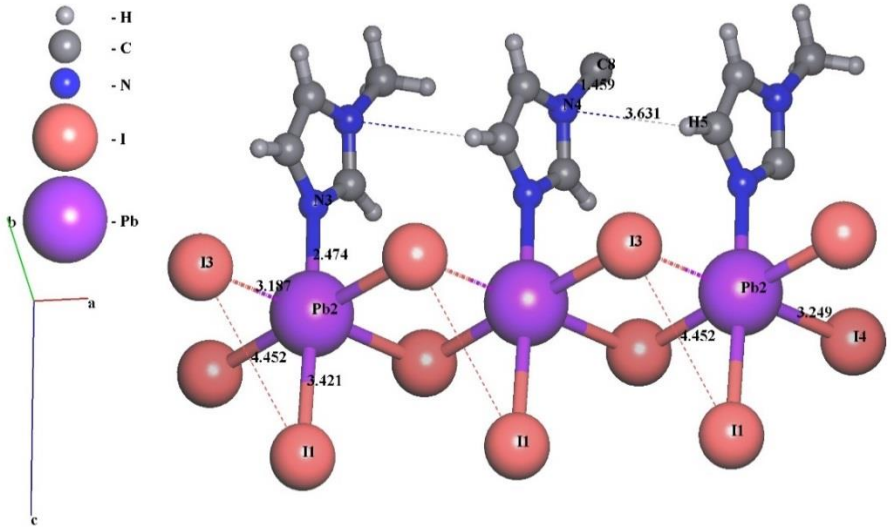

Figure 3. Bond distance in complex **1**.

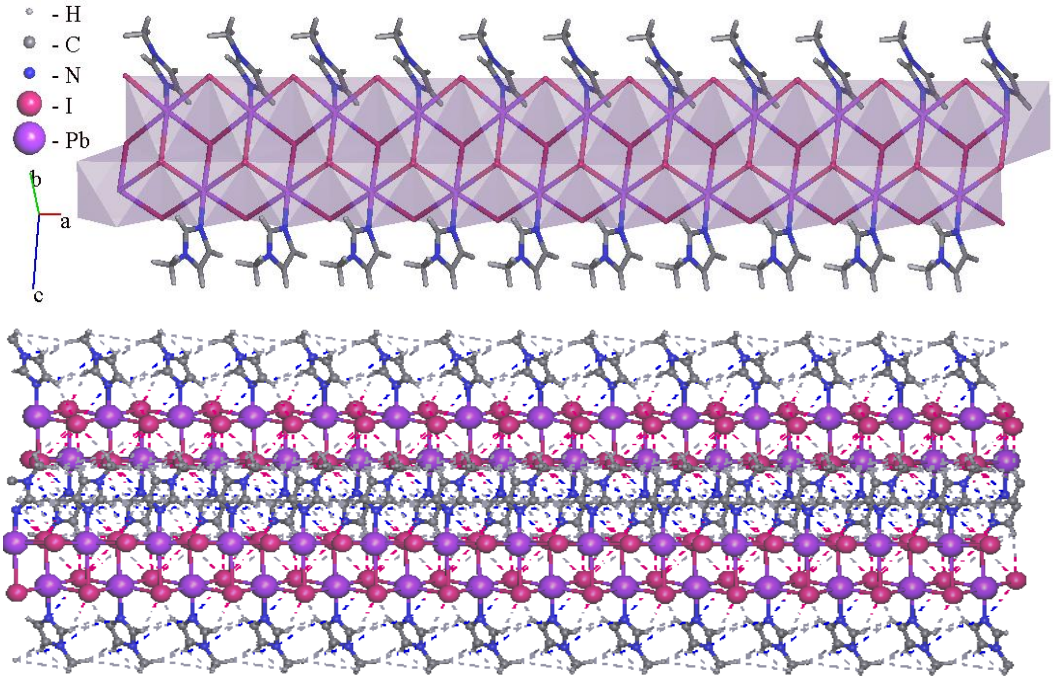

Figure 4. 1D chain of complex **1**(up) and interaction between chains (down).

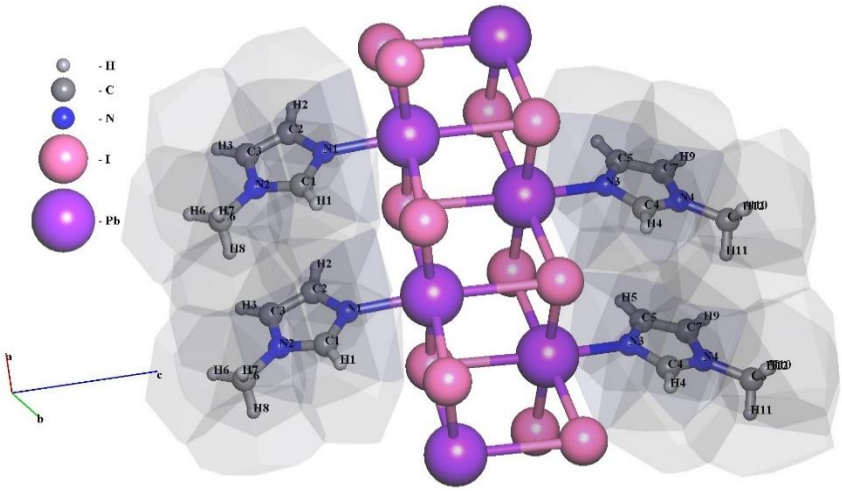

Figure 5. $\pi - \pi$ interaction in the *a* direction of the crystal.

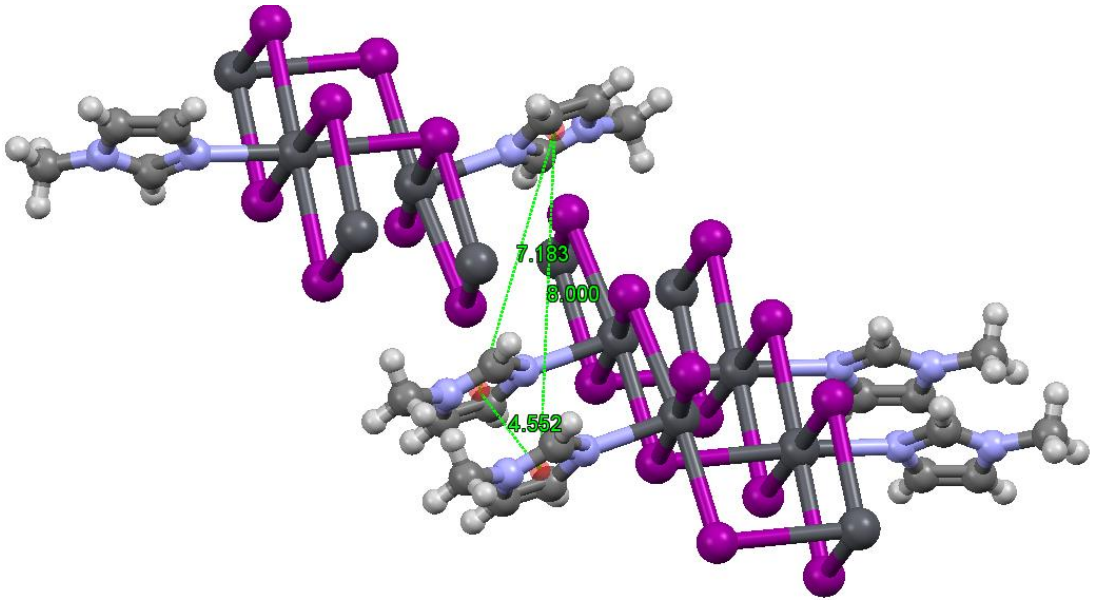

Figure 6. Distance between three parallel imidazole rings in the (101) plane.

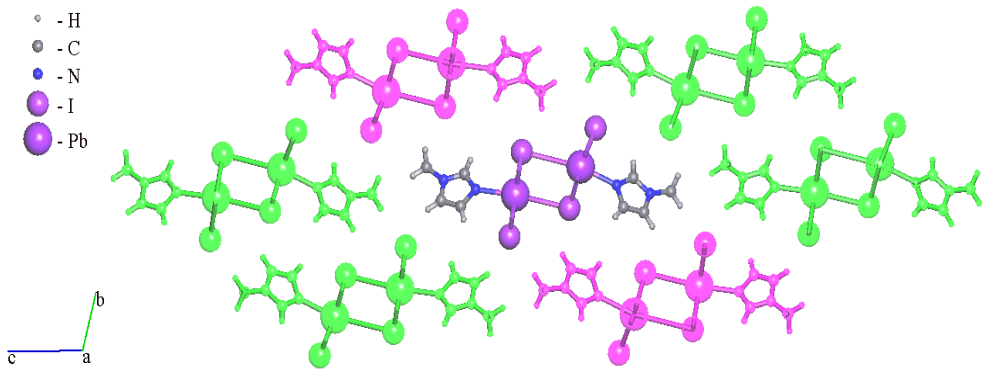

Figure 7. Alignment of the 1D chains along the [100] direction.

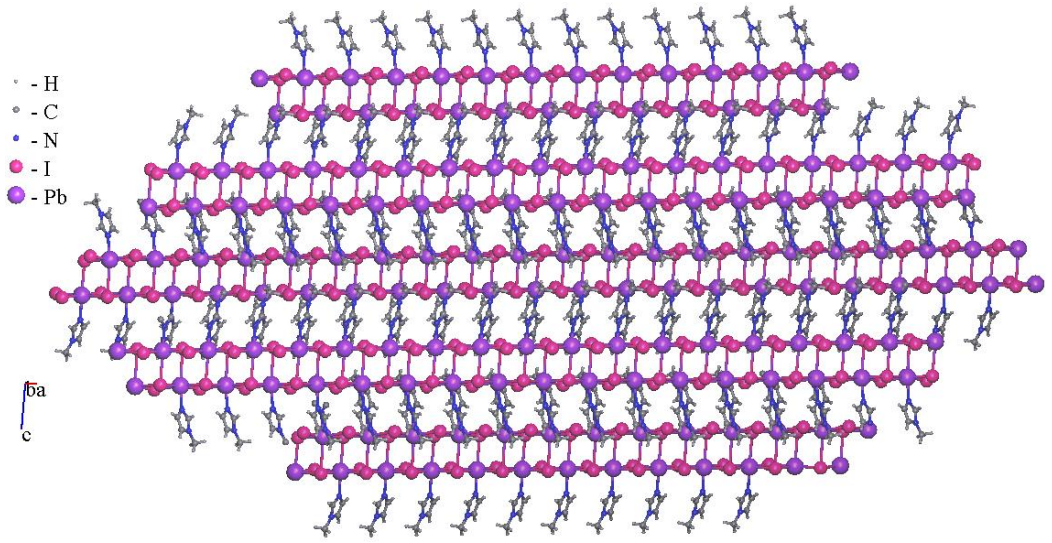

Figure 8. A fragment of the 3D framework in the [010] direction.

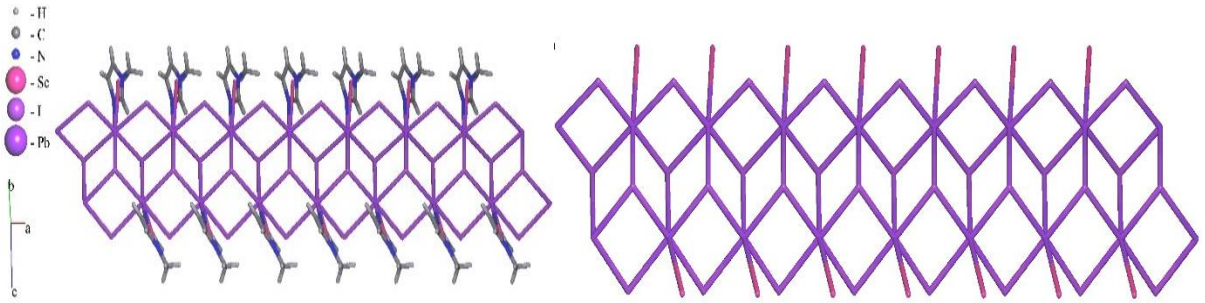

Figure 9. Topological representation of coordination networks.

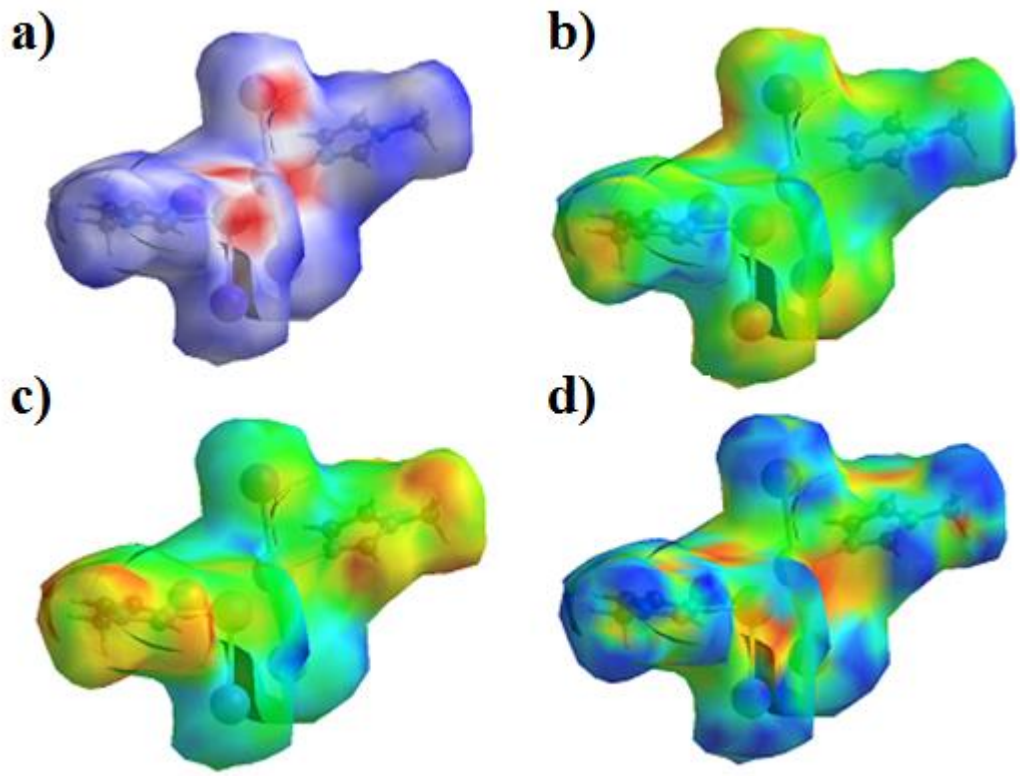

Figure 10. Hirshfeld surface analysis of **1**: a) Normalized distance (d_{norm}); b) distance from a point on the Hirshfeld surface to the nearest external nucleus (d_e); c) distance from a point on the Hirshfeld surface to the nearest internal nucleus (d_i); d) shape-index.

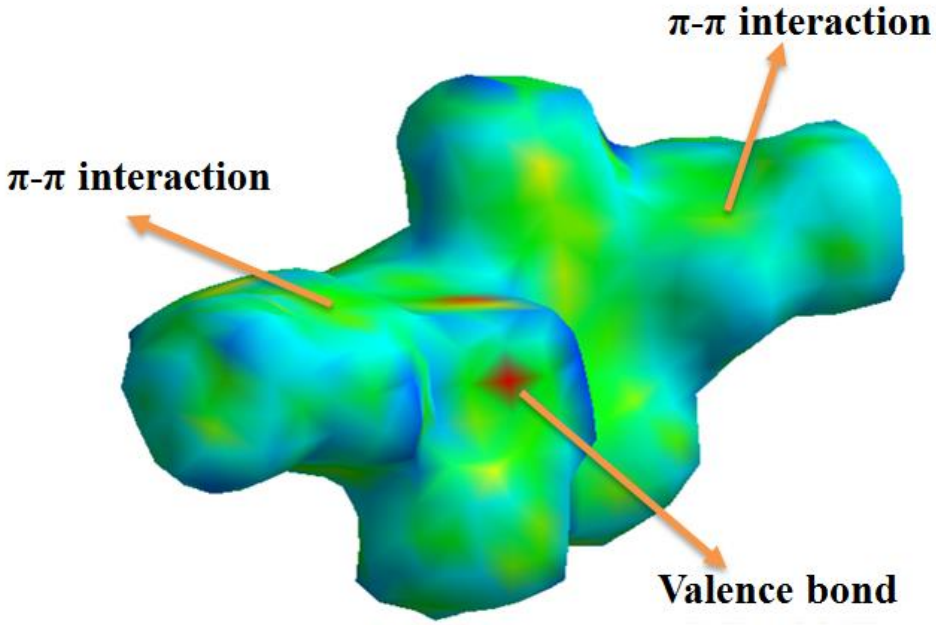

Figure 11. Hirshfeld surface of **1**.

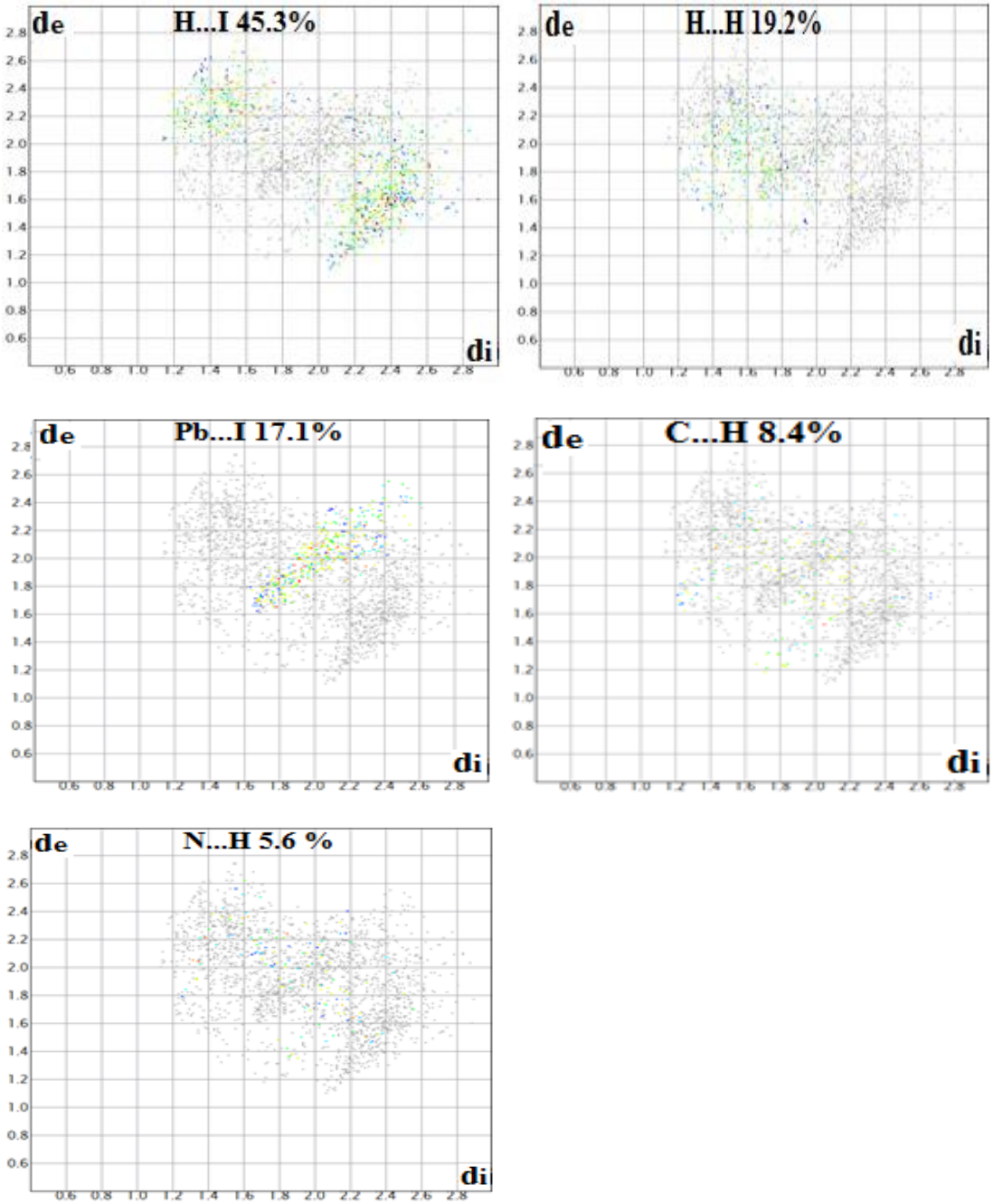

Figure 12. Fingerprint plots of major contacts in **1**.

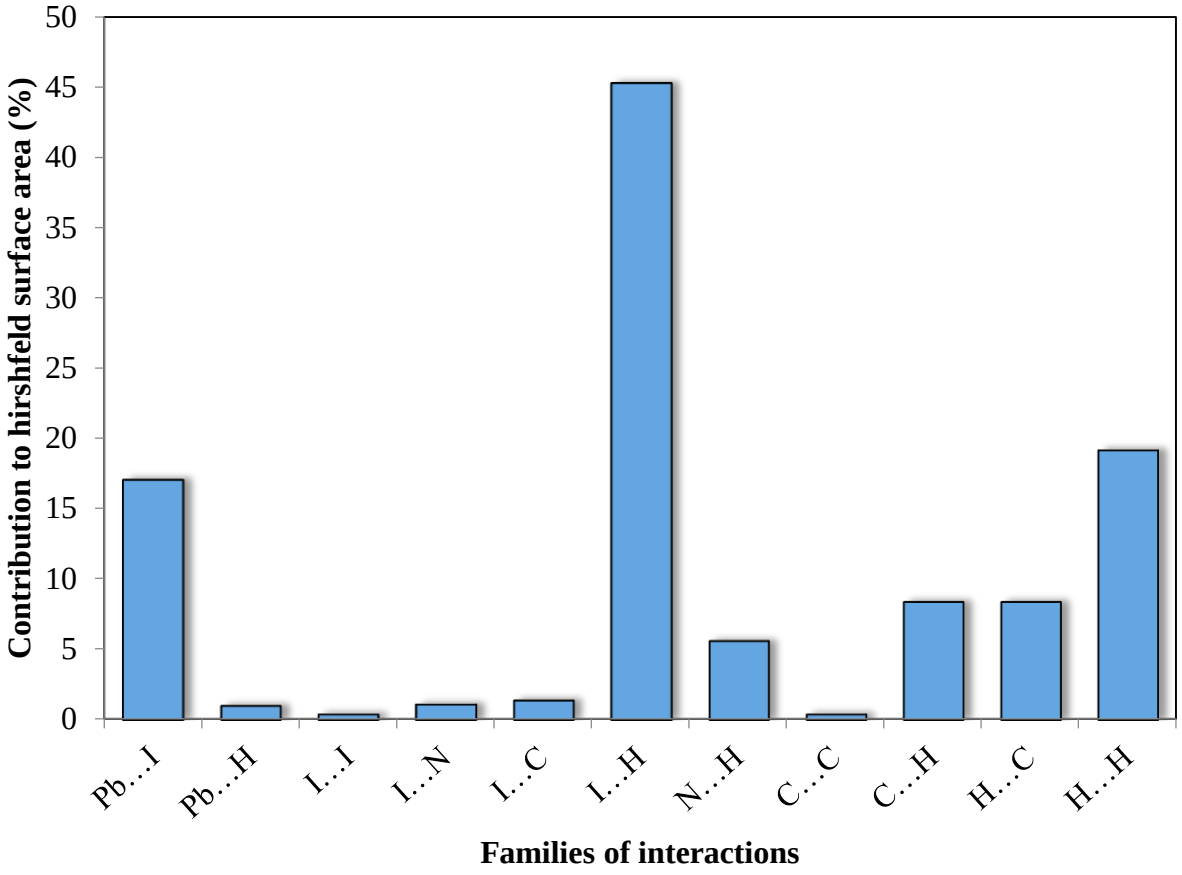

Figure 13. The relative contributions to the Hirshfeld surface area for **1**.

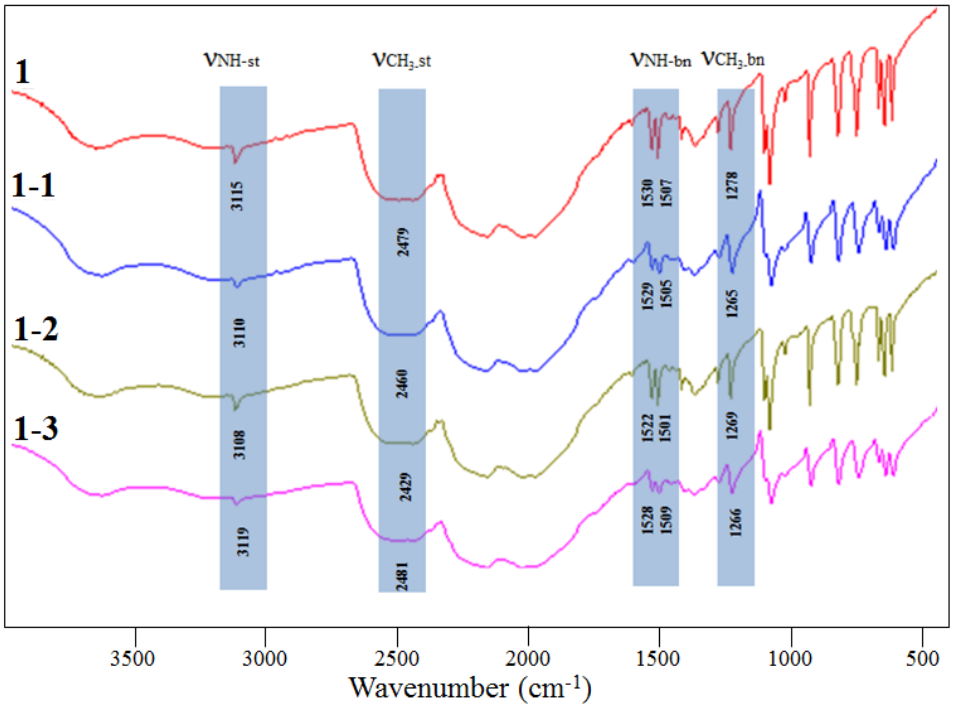

Figure 14. FT-IR spectra of nano-/microstructure 1, 1-1, 1-2 and 1-3.

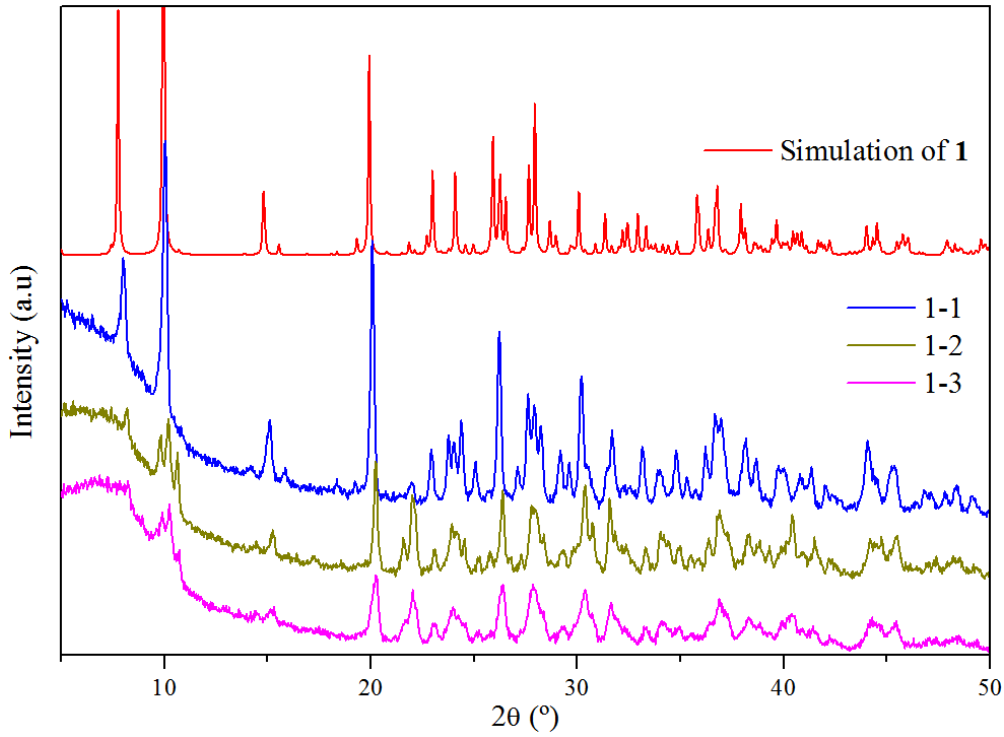

Figure 15. PXRD patterns corresponding to the simulation of complex **1** and the nano-/microstructure systems (**1-1**, **1-2** and **1-3**).

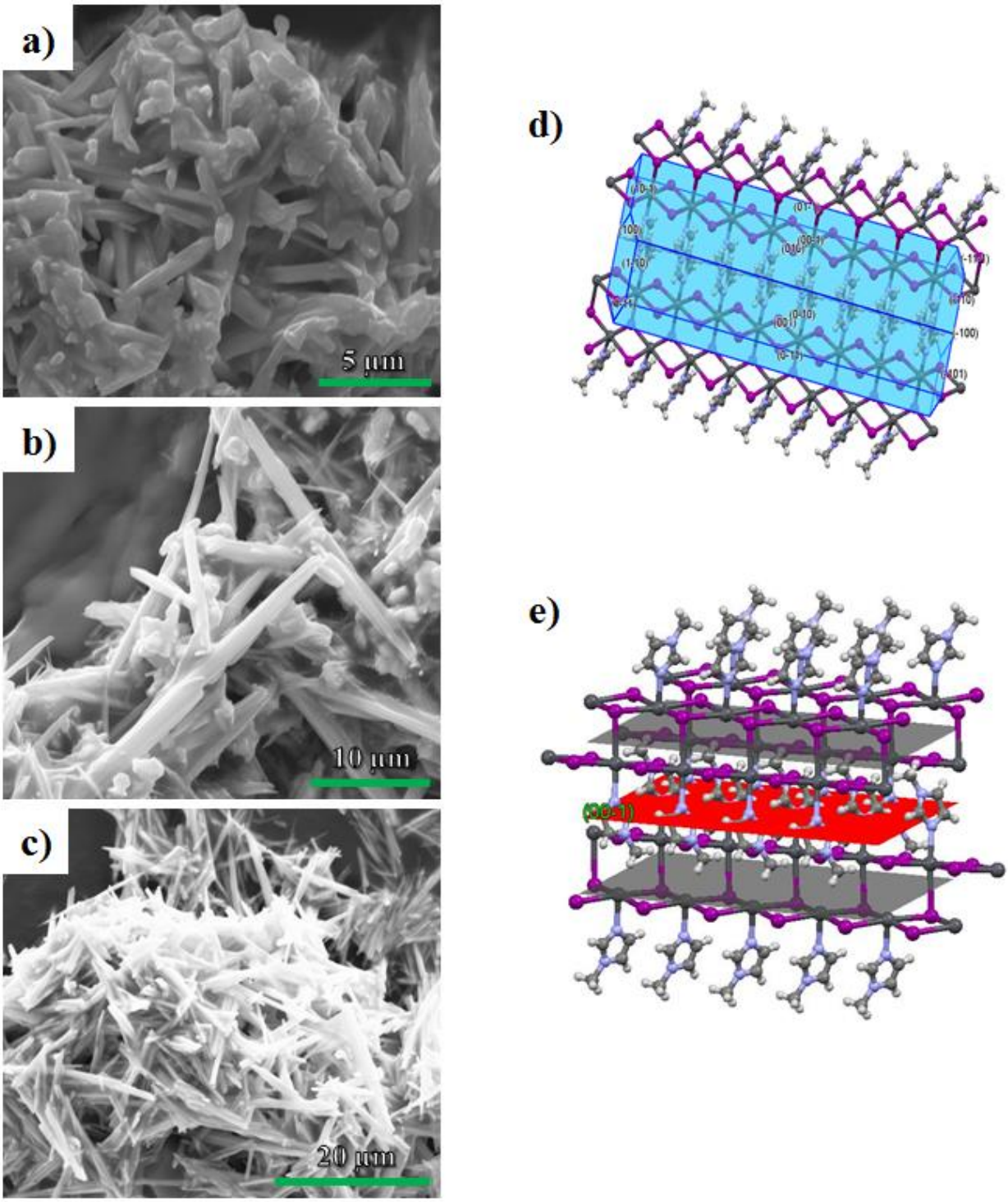

Figure 16. SEM image of the crystalline rods obtained in reaction: a) 1-1; b) 1-2 and c) 1-3; d) predicated needle crystal morphology of **1**, e) predicted from their packing along the [00-1] direction.